

Dalitz analysis of $B \rightarrow K\pi^+\psi'$ decays and the $Z(4430)^+$

R. Mizuk,¹⁴ I. Adachi,¹⁰ H. Aihara,⁴⁴ K. Arinstein,^{1,32} T. Aushev,^{19,14} A. M. Bakich,⁴¹ V. Balagura,¹⁴ E. Barberio,²² A. Bay,¹⁹ K. Belous,¹³ V. Bhardwaj,³⁴ A. Bozek,²⁸ M. Bračko,^{21,15} T. E. Browder,⁹ M.-C. Chang,⁵ A. Chen,²⁵ B. G. Cheon,⁸ C.-C. Chiang,²⁷ R. Chistov,¹⁴ I.-S. Cho,⁴⁹ S.-K. Choi,⁷ Y. Choi,⁴⁰ J. Dalseno,¹⁰ M. Danilov,¹⁴ S. Eidelman,^{1,32} N. Gabyshev,^{1,32} P. Goldenzweig,³ B. Golob,^{20,15} H. Ha,¹⁷ J. Haba,¹⁰ B.-Y. Han,¹⁷ T. Hara,¹⁰ Y. Hasegawa,³⁹ K. Hayasaka,²³ Y. Hoshi,⁴³ W.-S. Hou,²⁷ H. J. Hyun,¹⁸ T. Iijima,²³ K. Inami,²³ A. Ishikawa,³⁶ H. Ishino,^{45,*} R. Itoh,¹⁰ M. Iwasaki,⁴⁴ Y. Iwasaki,¹⁰ N. J. Joshi,⁴² D. H. Kah,¹⁸ J. H. Kang,⁴⁹ P. Kapusta,²⁸ H. Kawai,² T. Kawasaki,³⁰ H. J. Kim,¹⁸ H. O. Kim,¹⁸ J. H. Kim,⁴⁰ Y. I. Kim,¹⁸ Y. J. Kim,⁶ K. Kinoshita,³ B. R. Ko,¹⁷ S. Korpar,^{21,15} P. Križan,^{20,15} P. Krokovny,¹⁰ A. Kuzmin,^{1,32} Y.-J. Kwon,⁴⁹ S.-H. Kyeong,⁴⁹ J. S. Lange,⁵⁰ M. J. Lee,³⁸ S. E. Lee,³⁸ T. Lesiak,^{28,4} C. Liu,³⁷ Y. Liu,²³ D. Liventsev,¹⁴ R. Louvot,¹⁹ D. Marlow,³⁵ A. Matyja,²⁸ S. McOnie,⁴¹ K. Miyabayashi,²⁴ H. Miyata,³⁰ Y. Miyazaki,²³ T. Mori,²³ E. Nakano,³³ M. Nakao,¹⁰ H. Nakazawa,²⁵ Z. Natkaniec,²⁸ S. Nishida,¹⁰ O. Nitoh,⁴⁷ T. Ohshima,²³ S. Okuno,¹⁶ S. L. Olsen,⁹ P. Pakhlov,¹⁴ G. Pakhlova,¹⁴ C. W. Park,⁴⁰ H. Park,¹⁸ H. K. Park,¹⁸ R. Pestotnik,¹⁵ L. E. Piilonen,⁴⁸ H. Sahoo,⁹ K. Sakai,³⁰ Y. Sakai,¹⁰ O. Schneider,¹⁹ C. Schwanda,¹² A. Sekiya,²⁴ K. Senyo,²³ M. Shapkin,¹³ V. Shebalin,^{1,32} J.-G. Shiu,²⁷ B. Shwartz,^{1,32} S. Stanič,³¹ M. Starič,¹⁵ T. Sumiyoshi,⁴⁶ Y. Teramoto,³³ I. Tikhomirov,¹⁴ K. Trabelsi,¹⁰ S. Uehara,¹⁰ T. Uglov,¹⁴ Y. Unno,⁸ P. Urquijo,²² G. Varner,⁹ K. E. Varvell,⁴¹ K. Vervink,¹⁹ C. H. Wang,²⁶ M.-Z. Wang,²⁷ P. Wang,¹¹ X. L. Wang,¹¹ Y. Watanabe,¹⁶ R. Wedd,²² E. Won,¹⁷ B. D. Yabsley,⁴¹ Y. Yamashita,²⁹ C. Z. Yuan,¹¹ C. C. Zhang,¹¹ Z. P. Zhang,³⁷ V. Zhulanov,^{1,32} T. Zivko,¹⁵ A. Zupanc,¹⁵ and O. Zyukova^{1,32}

(The Belle Collaboration)

¹*Budker Institute of Nuclear Physics, Novosibirsk*

²*Chiba University, Chiba*

³*University of Cincinnati, Cincinnati, Ohio 45221*

⁴*T. Kościuszko Cracow University of Technology, Krakow*

⁵*Department of Physics, Fu Jen Catholic University, Taipei*

⁶*The Graduate University for Advanced Studies, Hayama*

⁷*Gyeongsang National University, Chinju*

⁸*Hanyang University, Seoul*

⁹*University of Hawaii, Honolulu, Hawaii 96822*

¹⁰*High Energy Accelerator Research Organization (KEK), Tsukuba*

¹¹*Institute of High Energy Physics, Chinese Academy of Sciences, Beijing*

¹²*Institute of High Energy Physics, Vienna*

¹³*Institute of High Energy Physics, Protvino*

¹⁴*Institute for Theoretical and Experimental Physics, Moscow*

¹⁵*J. Stefan Institute, Ljubljana*

¹⁶*Kanagawa University, Yokohama*

¹⁷*Korea University, Seoul*

¹⁸*Kyungpook National University, Taegu*

¹⁹*École Polytechnique Fédérale de Lausanne (EPFL), Lausanne*

²⁰*Faculty of Mathematics and Physics, University of Ljubljana, Ljubljana*

²¹*University of Maribor, Maribor*

²²*University of Melbourne, School of Physics, Victoria 3010*

²³*Nagoya University, Nagoya*

²⁴*Nara Women's University, Nara*

²⁵*National Central University, Chung-li*

²⁶*National United University, Miao Li*

²⁷*Department of Physics, National Taiwan University, Taipei*

²⁸*H. Niewodniczanski Institute of Nuclear Physics, Krakow*

²⁹*Nippon Dental University, Niigata*

³⁰*Niigata University, Niigata*

³¹*University of Nova Gorica, Nova Gorica*

³²*Novosibirsk State University, Novosibirsk*

³³*Osaka City University, Osaka*

³⁴*Panjab University, Chandigarh*

³⁵*Princeton University, Princeton, New Jersey 08544*

³⁶Saga University, Saga

³⁷University of Science and Technology of China, Hefei

³⁸Seoul National University, Seoul

³⁹Shinshu University, Nagano

⁴⁰Sungkyunkwan University, Suwon

⁴¹University of Sydney, Sydney, New South Wales

⁴²Tata Institute of Fundamental Research, Mumbai

⁴³Tohoku Gakuin University, Tagajo

⁴⁴Department of Physics, University of Tokyo, Tokyo

⁴⁵Tokyo Institute of Technology, Tokyo

⁴⁶Tokyo Metropolitan University, Tokyo

⁴⁷Tokyo University of Agriculture and Technology, Tokyo

⁴⁸IPNAS, Virginia Polytechnic Institute and State University, Blacksburg, Virginia 24061

⁴⁹Yonsei University, Seoul

⁵⁰Justus-Liebig-Universität Gießen, Gießen

From a Dalitz plot analysis of $B \rightarrow K\pi^+\psi'$ decays, we find a signal for $Z(4430)^+ \rightarrow \pi^+\psi'$ with a mass $M = (4443_{-12}^{+15+19}) \text{ MeV}/c^2$, width $\Gamma = (107_{-43}^{+86+74}) \text{ MeV}$, product branching fraction $\mathcal{B}(\bar{B}^0 \rightarrow K^- Z(4430)^+) \times \mathcal{B}(Z(4430)^+ \rightarrow \pi^+\psi') = (3.2_{-0.9}^{+1.8+5.3}) \times 10^{-5}$, and significance of 6.4σ that agrees with previous Belle measurements based on the same data sample. In addition, we determine the branching fraction $\mathcal{B}(B^0 \rightarrow K^*(892)^0\psi') = (5.52_{-0.32}^{+0.35+0.53}) \times 10^{-4}$ and the fraction of $K^*(892)^0$ mesons that are longitudinally polarized $f_L = (44.8_{-2.7}^{+4.0+4.0})\%$. These results are obtained from a 605 fb^{-1} data sample that contains 657 million $B\bar{B}$ pairs collected near the $\Upsilon(4S)$ resonance with the Belle detector at the KEKB asymmetric energy e^+e^- collider.

PACS numbers: 14.40.Gx, 12.39.Mk, 13.25.Hw

INTRODUCTION

In a paper on the B meson decay process $B \rightarrow K\pi^+\psi'$ [1], the Belle Collaboration [2] reported the observation of a distinct and relatively narrow peak in the $\pi^+\psi'$ mass spectrum near $M(\pi^+\psi') \simeq 4430 \text{ MeV}/c^2$. The analysis was performed by excluding the events in the $M(K\pi^+)$ regions of the $K^*(892)$ and $K^*(1430)$, and fitting the one-dimensional $M(\pi^+\psi')$ distribution. The fit gave a resonance mass and width of $M = (4433 \pm 4 \pm 2) \text{ MeV}/c^2$ and $\Gamma = (45_{-13}^{+18+30}) \text{ MeV}$, where the first uncertainty is statistical and the second is systematic; the significance of the resonance was 6.5σ . If this peak, called the $Z(4430)^+$, is interpreted as a meson state, then it must have an exotic structure; its minimal quark content is $|c\bar{c}u\bar{d}\rangle$.

The $Z(4430)^+$ observation motivated a subsequent Belle study of the process $\bar{B}^0 \rightarrow K^-\pi^+\chi_{c1}$, where a doubly peaked structure was observed in the $\pi^+\chi_{c1}$ invariant mass distribution [3]. In this channel, the observed structure is rather wide, therefore a full Dalitz plot analysis was used in order to establish that the observed peaks could be unambiguously associated with dynamics in the $\pi^+\chi_{c1}$ channel. If these peaks, called the $Z(4040)$ and $Z(4240)$, are attributed to meson states, a minimal four-quark substructure is required.

A recently reported study of $B \rightarrow K\pi^+\psi'$ decays by the BaBar Collaboration [4] did not find a significant signal for $Z(4430)^+ \rightarrow \pi^+\psi'$; the reported significance is at the $1.9\sigma - 3.1\sigma$ level. The BaBar sample of $B \rightarrow K\pi^+\psi'$ decays is about 85% the size of the corresponding

Belle data sample.

In this paper we present a reanalysis of the Belle $B \rightarrow K\pi^+\psi'$ data sample using a Dalitz plot formalism.

The Belle detector [5] is a large-solid-angle magnetic spectrometer that operates at the KEKB asymmetric-energy e^+e^- collider [6]. A data sample corresponding to an integrated luminosity of 605 fb^{-1} collected at the $\Upsilon(4S)$ resonance and containing 657 million $B\bar{B}$ pairs is used. A GEANT-based Monte Carlo (MC) simulation [7] is used to model the response of the detector.

EVENT SELECTION

We select events of the type $\bar{B}^0 \rightarrow K^-\pi^+\psi'$ and $B^+ \rightarrow K_S^0\pi^+\psi'$, where the ψ' decays either to $\ell^+\ell^-$ or $\pi^+\pi^-J/\psi$ with $J/\psi \rightarrow \ell^+\ell^-$ ($\ell = e$ or μ), $K_S^0 \rightarrow \pi^+\pi^-$. We use the same selection criteria as in Ref. [2]. In particular, we identify B mesons using the beam-energy constrained mass $M_{bc} = \sqrt{E_{\text{beam}}^2 - p_B^2}$ and the energy difference $\Delta E = E_{\text{beam}} - E_B$, where E_{beam} is the center-of-mass (c.m.) beam energy, p_B is the vector sum of the c.m. momenta of the B meson decay products and E_B is their c.m. energy sum. We select events with $|M_{bc} - m_B| < 7.1 \text{ MeV}/c^2$ (m_B is the world-average B -meson mass [8]) and $|\Delta E| < 34 \text{ MeV}$, which are both $\pm 2.5\sigma$ windows around the peak values. To model combinatorial backgrounds, we use events that are in the M_{bc} signal region and the ΔE sidebands defined as $|\Delta E \pm 70 \text{ MeV}| < 34 \text{ MeV}$. To improve the definition of the Dalitz plot boundaries for both signal and side-

band events, we perform a mass-constrained fit to the B candidates from both regions. Simulations of the two ψ' decay modes indicate that the experimental resolution for $M(\pi^+\psi')$ is $\sigma = 2.5 \text{ MeV}/c^2$ for both modes.

DALITZ PLOT DISTRIBUTION

We sum the Dalitz distributions for $\bar{B}^0 \rightarrow K^-\pi^+\psi'$ and $B^+ \rightarrow K_S^0\pi^+\psi'$ candidates. Due to the mass difference between K^- and K_S^0 the corresponding Dalitz plots have slightly different boundaries. We find that this has a negligible effect on the results of the Dalitz analysis. The Dalitz plot for the ΔE signal region is shown in Fig. 1. Here vertical bands corresponding to the $K^*(892)$ and the $K^*(1430)$ are evident. The horizontal cluster of entries in the vicinity of $M^2(\pi^+\psi') \sim 20 \text{ GeV}^2/c^4$ constitutes the $Z(4430)^+$ signal reported in Ref. [2].

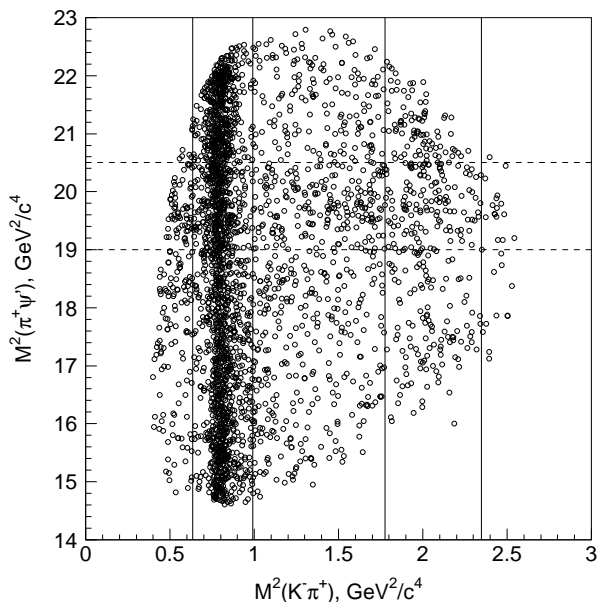


FIG. 1: The $B \rightarrow K\pi^+\psi'$ Dalitz plot for the ΔE signal region. The solid (dashed) lines delimit the five vertical (three horizontal) slices that are used to present the fit results in subsequent figures. The coordinates of the vertical lines are $M^2(K\pi^+) = (0.796)^2 \text{ GeV}^2/c^4$, $(0.996)^2 \text{ GeV}^2/c^4$, $(1.332)^2 \text{ GeV}^2/c^4$ and $(1.532)^2 \text{ GeV}^2/c^4$; the coordinates of the horizontal lines are $M^2(\pi^+\psi') = 19.0 \text{ GeV}^2/c^4$ and $20.5 \text{ GeV}^2/c^4$.

In the following, we illustrate the results of different fits using projected histograms of the slices of the Dalitz plot indicated by the vertical solid lines and horizontal dashed lines shown in Fig. 1. The three horizontal slices correspond to $M(\pi^+\psi')$ regions below, around and above the $Z(4430)^+$ mass region. The five vertical slices distinguish the $K^*(892)$ and $M(K\pi^+) \simeq 1.4 \text{ GeV}/c^2$ regions and bands above, below and in between them. The sum of the latter three projections corresponds to the K^* veto

used in Ref. [2].

FORMALISM OF THE DALITZ ANALYSIS

The decay $B \rightarrow K\pi^+\psi'$ with the ψ' reconstructed in the $\ell^+\ell^-$ decay mode is described by four variables (assuming the width of the ψ' to be negligible). These are taken to be $M(\pi^+\psi')$, $M(K\pi^+)$, the ψ' helicity angle (θ) and the angle between the ψ' production and decay planes (ϕ). In this analysis we integrate over the angular variables θ and ϕ . The MC indicates that the reconstruction efficiency is almost uniform over the full ϕ angular range; after integration over this angle the contribution from interference between the different ψ' helicity states is negligibly small. This allows the ψ' to be treated as a stable particle in the Dalitz analysis.

In the $\psi' \rightarrow \pi^+\pi^-J/\psi$ channel, the ψ' is likewise treated as stable. The $\pi^+\pi^-$ system in this decay is predominantly in an S -wave [9]; in this limit, the ψ' and J/ψ helicity states are the same, and we again find negligible interference contributions after integration over decay angles. Thus, our approach is the same as in the Dalitz analysis of the $\bar{B}^0 \rightarrow K^-\pi^+\chi_{c1}$ decays in Ref. [3].

The amplitude for the three-body decay $B \rightarrow K\pi^+\psi'$ is a sum over different quasi-two-body modes; resonances are described by relativistic Breit-Wigner functions with angular dependence. As the default fit model, we include all known low-lying $K\pi^+$ resonances [the κ or $K^*(800)$, and the $K^*(892)$, $K^*(1410)$, $K_0^*(1430)$, $K_2^*(1430)$, and $K^*(1680)$] and a single exotic $\pi^+\psi'$ resonance. In addition to the physics model, the fit function includes a background term derived from the ΔE sidebands and is modulated by the MC-determined experimental efficiency. The MC sample is generated using the world-average ψ' branching fractions [8] while to fix the relative fractions of the B^0 and B^+ contributions we use isospin symmetry. The Dalitz plots for the ΔE sideband and the MC sample are smoothed. The expression for the amplitudes, signal component of the fit function, and other details of the fitting procedure are the same as used in the analysis described in Ref. [3].

FIT RESULTS

The eight projected Dalitz plot slices with fit results for the default model superimposed are shown in Fig. 2. The $Z(4430)^+$ signal is most clearly seen in the third vertical slice. The sum of the 1st, 3rd and 5th vertical slices (*i.e.* a Dalitz plot projection with the K^* veto applied) is shown in Fig. 3. The $\pi^+\psi'$ resonance parameters determined from the fit are $M = (4443_{-12}^{+15}) \text{ MeV}/c^2$ and $\Gamma = (107_{-43}^{+86}) \text{ MeV}$. The central values agree well with the parameters reported in Ref. [2], while the errors are somewhat larger. The statistical significance, calculated

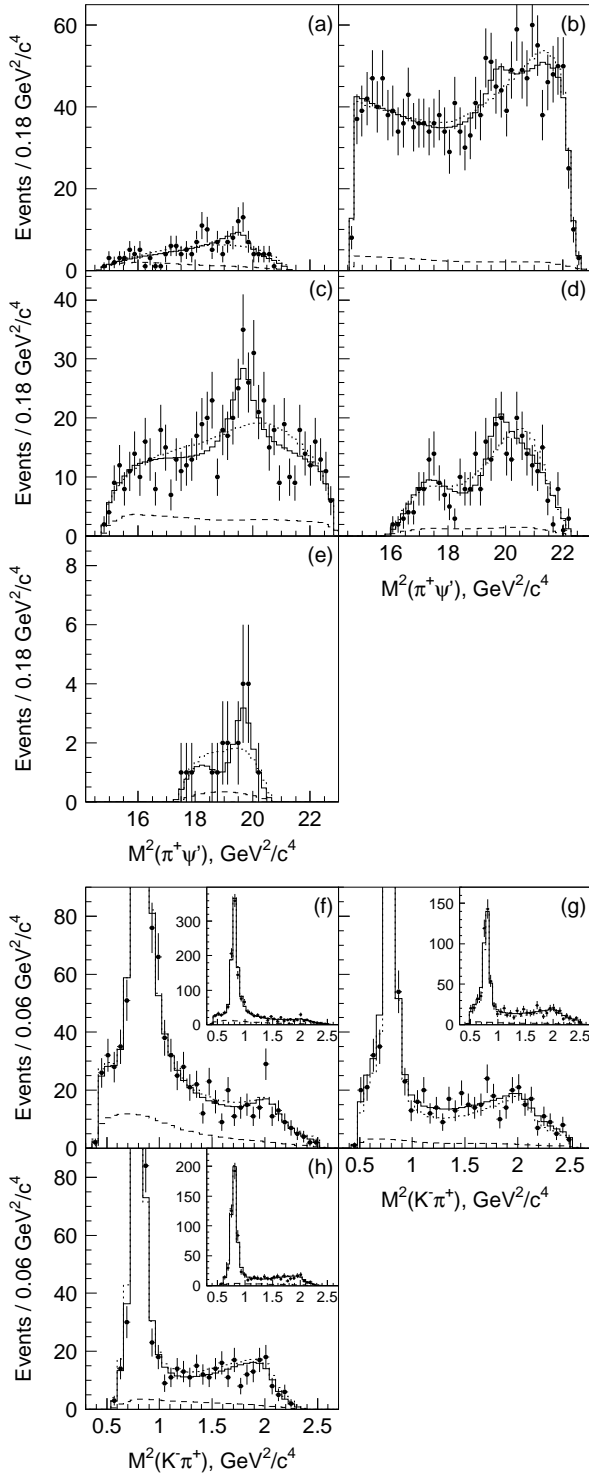


FIG. 2: Dalitz plot projections for the slices defined in Fig. 1: (a)-(e) correspond to vertical slices from left to right, (f)-(h) correspond to horizontal slices from bottom to top; in (f)-(h), plots including the full vertical scale are shown inset. The points with error bars represent data, the solid (dotted) histograms are the fit results for the default model that includes all low-lying $K\pi$ resonances and a single (without any) $\pi^+\psi'$ state, and the dashed histograms represent the background.

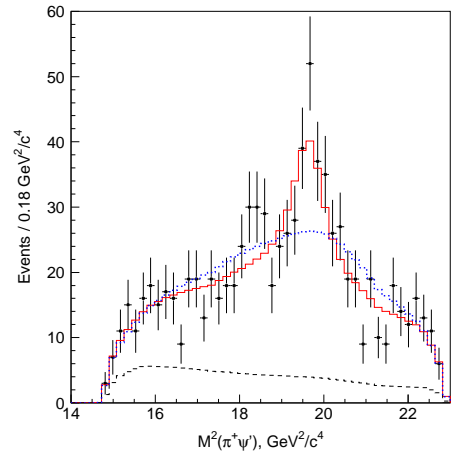


FIG. 3: The Dalitz plot projection with the K^* veto applied. The points with error bars represent data, the solid (dotted) histogram is the Dalitz plot fit result for the fit model with all $K\pi$ resonances and a single (without any) $\pi^+\psi'$ state, and the dashed histogram represents the background.

from the change in $2 \log \mathcal{L}$ when the $Z(4430)^+$ is included in the fit (taking the added degrees of freedom into account) is 6.4σ . The fit fractions and significances for all of the components are listed in Table I. The confidence

TABLE I: The fit fractions and significances of all contributions for the fit models with the default set of $K\pi^+$ resonances and a single $\pi^+\psi'$ resonance.

Contribution	Fit fraction (%)	Significance
$Z(4430)^+$	$5.7^{+3.1}_{-1.6}$	6.4σ
κ	$4.1^{+3.4}_{-1.1}$	1.5σ
$K^*(892)$	$64.8^{+3.8}_{-3.5}$	large
$K^*(1410)$	$5.5^{+8.8}_{-1.5}$	0.5σ
$K_0^*(1430)$	5.3 ± 2.6	1.3σ
$K_2^*(1430)$	$5.5^{+1.6}_{-1.4}$	3.1σ
$K^*(1680)$	$2.8^{+5.8}_{-1.0}$	1.2σ

level (C.L.) of the fit model with (without) the $Z(4430)^+$ is 36% (0.1%). The C.L.'s are determined using ensembles of the MC simulated experiments.

To study the model dependence, we consider a variety of other fit hypotheses. These include: successively removing each K^* resonance component; adding, for each case, a non-resonant phase-space term; relaxing the constraints on the κ mass and width; replacing the κ with the LASS group's parameterization for the $K\pi$ S -wave amplitude [11], and including another $J = 1$ ($J = 2$) K^* resonance with mass and width left as free parameters. The lowest $Z(4430)^+$ significance of 5.4σ corresponds to the model with a non-resonant phase-space term and a new $J = 2$ K^* resonance. We treat the maximum varia-

tion of the $Z(4430)^+$ parameters from these different fit models as the systematic uncertainty. The resulting uncertainty estimates are given in the first row of Table II.

We find the uncertainty due to the variation of the r parameter in the Blatt-Weisskopf form factors [10] to be negligible. The contribution of the uncertainties in the mass and width of intermediate K^* resonances that are fixed in the fit is also found to be negligible.

We vary the assumption about the value of the B decay orbital angular momentum (L) for those cases where several possibilities exist. The resulting uncertainties are given in the second row in Table II.

In the fits described above, the spin of the $Z(4430)^+$ is assumed to be zero. We find that the $J = 1$ assumption does not significantly improve the fit quality. The variations in the $Z(4430)^+$ parameters for the different spin assignments are considered as systematic uncertainties and are listed in the third row in Table II.

We consider alternative smoothing procedures for ΔE sidebands and MC samples. The corresponding variation of the $Z(4430)^+$ parameters are given in the fourth row in Table II.

To obtain the total systematic uncertainties, the values given in Table II are added in quadrature. The resulting mass, width and fit fraction are $M = (4443^{+15+19}_{-12-13}) \text{ MeV}/c^2$, $\Gamma = (107^{+86+74}_{-43-56}) \text{ MeV}$, $f = (5.7^{+3.1+9.4}_{-1.6-2.7})\%$.

TABLE II: Systematic uncertainties in the $Z(4430)^+$ mass, width and fit fraction due to various sources.

	$M, \text{ MeV}/c^2$	$\Gamma, \text{ MeV}$	Fit fraction, %
Fit model	+14 -13	+56 -52	+3.6 -2.7
L assignment	+8 -0	+44 -0	+2.0 -0.0
Z spin assignment	+9 -0	+8 -0	+8.4 -0
Smoothing procedure	+4 -3	+17 -23	+0.5 -0.2

OTHER FITS

In principle, more complex mass structures can be produced by reflections from higher $K\pi^+$ partial waves. To examine this, we perform the Dalitz plot fit with a $K_3^*(1780)$ resonance term added to the default model (see Fig. 4). In this case, the $Z(4430)^+$ signal persists with mass and width within 1σ of their default model values and with a statistical significance of 4.7σ . However, the $K_3^*(1780)$ fit fractions — 6.8% and 6.6% for the $Z(4430)^+$ and non- $Z(4430)^+$ hypotheses, respectively — are very large for a resonance with a peak mass that is $\sim 180 \text{ MeV}/c^2$ ($\simeq 1.2\Gamma_{K_3^*(1780)}$) above the kinematic limit for $B \rightarrow K\pi^+\psi'$ decays and for which only a small portion of the low-mass tail of the resonance is accessible.

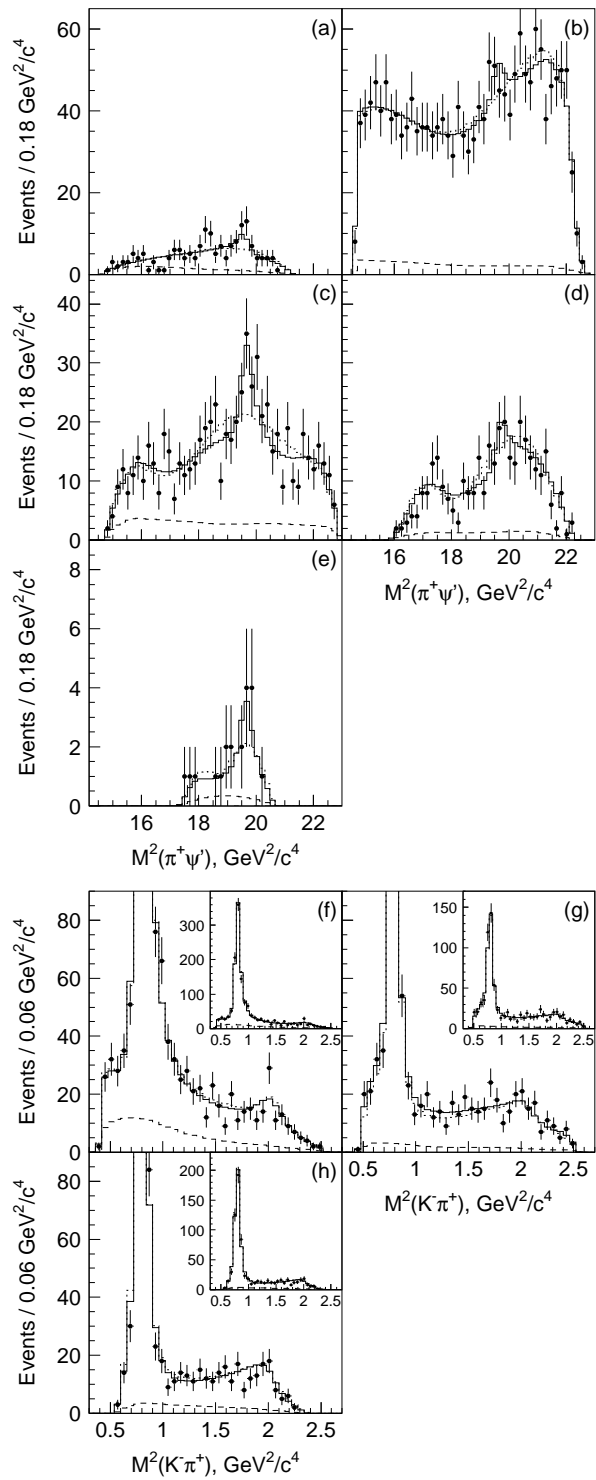


FIG. 4: Dalitz plot projections as described for Fig. 2. The points with error bars represent data, the solid (dotted) histograms are the fit results for the model that includes all low-lying $K\pi$ resonances as well as the $K_3^*(1780)$ and a single (without any) $\pi^+\psi'$ state, and the dashed histograms represent the background.

Moreover $B \rightarrow K_3^*(1780)\psi'$ decay has an $L \geq 2$ centrifugal barrier and the $K_3^*(1780) \rightarrow K\pi$ branching fraction is only $(18.8 \pm 1.0)\%$ [8]. For these reasons, the 4.7σ significance estimate from this fit model is likely to be an underestimate of the real value. Studies of other B decays where the $K_3^*(1780)$ can contribute (e.g. $B \rightarrow K\pi^+J/\psi$ and $B \rightarrow K^*\pi^+\psi'$) may provide further insight. The C.L. of the default model with an additional contribution from the $K_3^*(1780)$ is 58% (6%) for the $Z(4430)^+$ (non- $Z(4430)^+$) hypothesis. The significant $Z(4430)^+$ contribution is concentrated in a small area of the Dalitz plot.

If a second Z state is added to the fit, we find a mass $M \sim 4.3 \text{ GeV}/c^2$ and a width $\Gamma \sim 0.2 \text{ GeV}$, with a significance of 3.9σ .

Angular distributions for ψ' decays can be predicted based on the Dalitz plot fit results and therefore provide a useful cross-check (see Ref. [3] for details). We find good agreement between data and predictions for various fit models. The statistics are not sufficient to discriminate between models in our approach.

BRANCHING FRACTIONS

To measure branching fractions we use only $\bar{B}^0 \rightarrow K^-\pi^+\psi'$ decays. The yields of these decays with the ψ' reconstructed in the $\ell^+\ell^-$ and $\pi^+\pi^-J/\psi$ channels are found from fits to the ΔE distributions to be 1089 ± 34 and 1166 ± 37 , respectively.

To determine the experimental efficiency, we used the phase-space MC events weighted according to the results of the Dalitz plot fit. The efficiencies are $(19.2 \pm 1.4)\%$ and $(8.2 \pm 0.7)\%$ for $\psi' \rightarrow \ell^+\ell^-$ and $\psi' \rightarrow \pi^+\pi^-J/\psi$ channels, respectively. The uncertainties include the dependence on the Dalitz plot model (0.1%); data and MC differences for track reconstruction (1% per track), and particle identification (4% for the $K^-\pi^+$ pair and 4.2% for $\ell^+\ell^-$); and MC statistics (0.6%). The uncertainties from different sources are added in quadrature. The efficiencies are corrected for the difference in lepton identification performance in data compared to MC, $(-4.5 \pm 4.2)\%$, determined from $J/\psi \rightarrow \ell^+\ell^-$ and $e^+e^- \rightarrow e^+e^-\ell^+\ell^-$ control samples.

Using $(656.7 \pm 8.9) \times 10^6/2$ as the number of $B^0\bar{B}^0$ pairs and world-average values for the intermediate branching fractions [8], we determine $\mathcal{B}(\bar{B}^0 \rightarrow K^-\pi^+\psi') = (5.68 \pm 0.13 \pm 0.42) \times 10^{-4}$. This value is in agreement with BaBar's value $(5.57 \pm 0.16) \times 10^{-4}$ [4] (statistical error only). The branching fractions calculated for the two ψ' decay channels are in good agreement: $(5.73 \pm 0.18) \times 10^{-4}$ and $(5.62 \pm 0.18) \times 10^{-4}$ (statistical errors only). The systematic error includes contributions from the uncertainties in the efficiencies and the branching fractions of the intermediate resonances.

Based on the $Z(4430)^+$ fit fraction we find a prod-

uct branching fraction $\mathcal{B}(\bar{B}^0 \rightarrow K^-Z(4430)^+) \times \mathcal{B}(Z(4430)^+ \rightarrow \pi^+\psi') = (3.2_{-0.9}^{+1.8+5.3}) \times 10^{-5}$. This is in agreement with the previous Belle result [2] and consistent with the BaBar upper limit of 3.1×10^{-5} [4].

The dominant feature of the $B \rightarrow K\pi^+\psi'$ decay process is the $B \rightarrow K^*(892)\psi'$ intermediate state. Using the fit fraction from Table I, and evaluating systematic errors using the same procedure as for the $Z(4430)^+$ measurements, we determine the branching fraction $\mathcal{B}(B^0 \rightarrow K^*(892)^0\psi') = (5.52_{-0.32-0.58}^{+0.35+0.53}) \times 10^{-4}$ and the fraction of $K^*(892)^0$ mesons that are longitudinally polarized $f_L = (44.8_{-2.7-5.3}^{+4.0+4.0})\%$. The branching fraction is somewhat below the world-average value of $(7.2 \pm 0.8) \times 10^{-4}$ [8]; the longitudinal polarization fraction agrees with the CLEOII result of $0.45 \pm 0.11 \pm 0.04$ and has better precision [12].

CONCLUSIONS

From a Dalitz plot analysis of $B \rightarrow K\pi^+\psi'$ decays, we find a signal for $Z(4430)^+ \rightarrow \pi^+\psi'$ with a mass $M = (4443_{-12-13}^{+15+19}) \text{ MeV}/c^2$, width $\Gamma = (107_{-43-56}^{+86+74}) \text{ MeV}$ and product branching fraction $\mathcal{B}(\bar{B}^0 \rightarrow K^-Z(4430)^+) \times \mathcal{B}(Z(4430)^+ \rightarrow \pi^+\psi') = (3.2_{-0.9-1.6}^{+1.8+5.3}) \times 10^{-5}$. The statistical significance of this signal is 6.4σ ; the significance including systematic uncertainty from the fit models is 5.4σ . These results agree with, and supersede previous measurements based on the same data sample reported in Ref. [2].

In addition we determine the branching fraction $\mathcal{B}(B^0 \rightarrow K^*(892)^0\psi') = (5.52_{-0.32-0.58}^{+0.35+0.53}) \times 10^{-4}$ and the fraction of $K^*(892)$ mesons that are longitudinally polarized $f_L = (44.8_{-2.7-5.3}^{+4.0+4.0})\%$. These are the first measurements of these quantities that are derived from a Dalitz plot analysis.

Acknowledgments

We thank the KEKB group for excellent operation of the accelerator, the KEK cryogenics group for efficient solenoid operations, and the KEK computer group and the NII for valuable computing and SINET3 network support. We acknowledge support from MEXT, JSPS and Nagoya's TLPRC (Japan); ARC and DIISR (Australia); NSFC (China); DST (India); MEST, KOSEF, KRF (Korea); MNiSW (Poland); MES and RFAAE (Russia); ARRS (Slovenia); SNSF (Switzerland); NSC and MOE (Taiwan); and DOE (USA).

* now at Okayama University, Okayama

[1] The inclusion of charge-conjugate modes is implied throughout this paper. By ψ' we mean the $\psi(3686)$, also known as the $\psi(2S)$.

- [2] S.-K. Choi *et al.* (Belle Collaboration), Phys. Rev. Lett. **100**, 142001 (2008).
- [3] R. Mizuk *et al.* (Belle Collaboration), Phys. Rev. D **78**, 072004 (2008).
- [4] B. Aubert *et al.* (BaBar Collaboration), arXiv:0811.0564 [hep-ex].
- [5] A. Abashian *et al.* (Belle Collaboration), Nucl. Instrum. Methods Phys. Res., Sect. A **499**, 1 (2003).
- [6] S. Kurokawa and E. Kikutani, Nucl. Instrum. Methods Phys. Res., Sect. A **479**, 117 (2002), and other papers included in this volume.
- [7] R. Brun *et al.*, GEANT 3.21, CERN DD/EE/84-1, 1984.
- [8] C. Amsler *et al.* (Particle Data Group), Phys. Lett.B **667**, 1 (2008).
- [9] J.Z. Bai *et al.* (BES Collaboration), Phys. Rev. D **62**, 032002 (2000).
- [10] J. Blatt and V. Weisskopf, Theoretical Nuclear Physics, p.361, New York: John Wiley & Sons (1952).
- [11] D. Aston *et al.* (LASS Collaboration), Nucl. Phys. B **296**, 493 (1988).
- [12] S. J. Richichi *et al.* (CLEO Collaboration), Phys. Rev. D **63**, 031103 (2001).